

Dual Reinforcement-Based Specification Generation for Image De-Rendering

Ramakanth Pasunuru^{*} David Rosenberg[†] Gideon Mann[†] Mohit Bansal^{*}

UNC Chapel Hill^{*} Bloomberg LP[†]
 {ram, mbansal}@cs.unc.edu

{drosenberg44, gmann16}@bloomberg.net

Abstract

Advances in deep learning have led to promising progress in inferring graphics programs by de-rendering computer-generated images. However, current methods do not explore which decoding methods lead to better inductive bias for inferring graphics programs. In our work, we first explore the effectiveness of LSTM-RNN versus Transformer networks as decoders for order-independent graphics programs. Since these are sequence models, we must choose an ordering of the objects in the graphics programs for likelihood training. We found that the LSTM performance was highly sensitive to the sequence ordering (random order vs. pattern-based order), while Transformer performance was roughly independent of the sequence ordering. Further, we present a policy gradient based reinforcement learning approach for better inductive bias in the decoder via multiple diverse rewards based both on the graphics program specification and the rendered image. We also explore the combination of these complementary rewards. We achieve state-of-the-art results on two graphics program generation datasets.

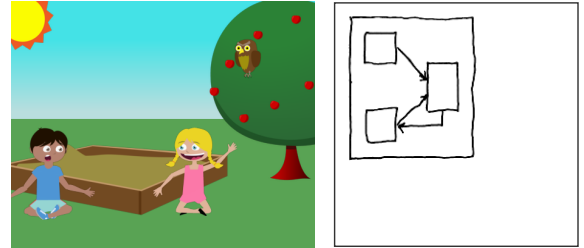
1 Introduction

The large majority of computer vision work deals in the domain of natural images or video. However, there is tremendous potential for applying computer vision techniques to computer-generated images, such as plots, charts, schematics, complicated math formulas, and even a page of printed text. For these domains, there is often a domain-specific language for precisely specifying the image, such as matplotlib code for a chart, PicTeX for a schematic¹, and LaTeX for math formulas and text. “De-rendering” a computer-generated image back to the original (or a different) domain-specific language specification can be a useful first step in many tasks, such as changing the visual appearance of an image (Huang et al. 2016; Wu, Tenenbaum, and Kohli 2017) or extracting information contained in an image (Cliche et al. 2017; Mishchenko and Vassilieva 2011).

The de-rendering problem is part of a larger class of “image-to-text” problems, in which an input image is

Copyright © 2021 for this paper by its authors. Use permitted under Creative Commons License Attribution 4.0 International (CC BY 4.0).

¹<https://ctan.org/pkg/pictex?lang=en>



```
<object>
  <supercategory>C-1</supercategory>
  <category>CS-3</category>
  <x-coordinate>120</x-coordinate>
  <y-coordinate>240</y-coordinate>
  <depth>1</depth>
  <flip>0</flip>
</object>
<object>....
```

```
<object>
  <category>Rectangle</category>
  <x1-coordinate>7</x1-coordinate>
  <y1-coordinate>1</y1-coordinate>
  <x2-coordinate>11</x2-coordinate>
  <y2-coordinate>16</y2-coordinate>
</object>
<object>....
```

Figure 1: Example images from the abstract scene dataset (left) and the Noisy Shapes dataset (right), along with portions of their specifications.

mapped to some sequence of output tokens. The neural encoder-decoder approach has proved to be very successful for this class of problems, including image captioning (Karpathy and Fei-Fei 2015; Xu et al. 2015), handwriting recognition (Bluche, Louradour, and Messina 2016), as well as the de-rendering problem for math formulas (Deng et al. 2017) and graphics images (Ellis et al. 2018; Wu, Tenenbaum, and Kohli 2017). In this paper, we improve these encoder-decoder models for the specific case of graphical images, via methods based on Transformer models with both cross-entropy training and reinforcement learning with up to two “dual modality” reward functions. De-rendering graphical images is a problem that differs in several interesting ways from image captioning and OCR problems. Two examples of the de-rendering problem we consider are shown in Fig. 1. Each image is an input, and a portion of the desired output is displayed below each image. In de-rendering, every object in the image must be described in the specification, and typically many output tokens are required to describe each object. Thus outputs from de-rendering are typically much longer than those in image captioning datasets (Chen

et al. 2015), since caption labels (e.g., in COCO (Lin et al. 2014)) tend to focus on simple descriptions involving only the most salient objects in the image. OCR and de-rendering are similar in that they encode information about all elements of the image, but the order of the output sequence in OCR is completely determined by the image, while in de-rendering, the output sequences represent sets², and as such the final rendering is invariant to a large degree of reordering in the output sequence (e.g., by shuffling the sub-sequences of tokens that correspond to separate objects).

We start our investigation with a basic image captioning model (similar to Wu, Tenenbaum, and Kohli (2017)) and extend it with an attention mechanism. We then swap out the LSTM-RNN decoder with a Transformer network (Vaswani et al. 2017). Our original motivation for this replacement is that we think that output generation requires long-term dependencies to avoid representing the same object multiple times. As mentioned above, de-rendered output sequences can be quite long, and we thought the multi-head attention mechanism of the Transformer would handle the long-range dependencies better than the LSTM-RNN. Unexpectedly, we found another advantage of Transformers over LSTM-RNNs for handling output sequence that can be reordered in many ways and still be correct. We expand on this in Sec. 7.1. To our knowledge, we are the first ones to use Transformer networks for de-rendering graphical images, and we find this change is a significant source of our performance improvement.

Another challenge with graphics de-rendering is that changing one or a few tokens in the specification can cause a significant change in many pixel values (e.g., by changing the location or color of a large object). Conversely, one can have two images that are very close visually, yet have completely different specifications. To this end, we explore the error minimization in the image as well as the specification space via a dual-modality, two-way reward reinforcement learning approach (Williams 1992; Zaremba and Sutskever 2015). We train with non-differentiable reward functions that reflect performance measures of interest in both the image space and the specification space (the “dual modes”). We further explore training a single model using rewards from both modalities, with the hopes that we get complementary feedback from each.

We empirically evaluate our methods on two image de-rendering datasets: Noisy Shapes dataset (Ellis et al. 2018) and Abstract Scene dataset (Zitnick and Parikh 2013; Wu, Tenenbaum, and Kohli 2017). Our Transformer models trained with cross-entropy loss achieve very significant improvement over previous work on these datasets. We show even more improvement when we train the Transformer models using policy gradients-based methods, both via single-modality rewards and further improvements via dual-modality joint rewards. Finally, in our analysis we find evidence that the performance of Transformers is relatively insensitive to the ordering of objects in the output sequence, while the performance of LSTM-RNN’s can decay substan-

²We say sets, rather than sequences, because in our datasets object ordering does not affect the rendering.

tially for a poorly chosen object ordering. This suggests that the advantage of Transformers over LSTM-RNNs may be particularly strong in tasks where we are using an output sequence to represent an unordered set of objects.

2 Related Work

De-rendering a computer-generated image to a domain-specific language provides an abstraction that is easy to change, store, compare and match to other images. As a consequence, there has been recent interest and work in this area. Huang et al. (2016) used CNNs to translate a hand-drawn sketch of an object (e.g., jewellery) to a fixed set of parameters for a procedural model. In a similar vein, Nishida et al. (2016) proposed a simple procedural grammar as a building block to turn sketches into realistic 3D models. Ellis et al. (2018) proposed an automatic visual program induction model to infer programs from hand-drawn images, where the images are encoded via CNNs and a multi-layer perceptron predicts a distribution over drawing commands.

Ha and Eck (2018) presented a recurrent neural network based sketch-rnn to construct conditional and unconditional sketch generation of common objects, constrained by a very simple set of primitives. Their model describes images as pen movements either in a drawing mode or in a non-drawing mode. Unlike our approach, this program is highly sequence dependent and non-compositional. While there are different solutions to the problem by re-ordering, one cannot arbitrarily shuffle the sequence of pen movements. Liu et al. (2019) infer scene programs by exploiting hierarchical object-based scene representations. Sun et al. (2018) proposed a neural program synthesizer that generates underlying programs for behaviorally diverse demonstration videos. In this work, we use Transformer networks (Vaswani et al. 2017) for decoding the specification from the given input image. Transformers have been used in other generation tasks such as image and video captioning (Sharma et al. 2018; Zhou et al. 2018), however, we are the first ones to use Transformer networks for the image de-rendering problem. Vinyals, Bengio, and Kudlur (2015) shows that an LSTM trained with shuffled targets (unordered) using cross-entropy has a substantial drop in performance compared to natural orderings. Our result supports their findings and moreover we find that Transformers, by contrast, are relatively insensitive to the ordering of the objects.

Recently, policy gradient-based reinforcement learning (RL) methods have been widely used for sequence generation tasks: machine translation (Ranzato et al. 2016), image captioning (Ranzato et al. 2016; Rennie et al. 2017), and textual summarization (Paulus, Xiong, and Socher 2018; Pasunuru and Bansal 2018). Daumé, Langford, and Marcu (2009) proposed to improve sequence generation by allowing a model to use its own prediction at training time, extending their work in structured prediction. In the context of program synthesis, Bunel et al. (2018) used RL for generating semantically correct programs. In the context of image de-rendering, Wu, Tenenbaum, and Kohli (2017) proposed a neural scene de-rendering model (NSD) with a neural encoder and a graphics engine as a decoder. The encoder has an object proposal generator that produces segment proposals,

and then it tries to interpret objects and their properties from these segments. They use RL to better sample the proposals and use the rendered image reconstruction error as reward.

Recently, Ganin et al. (2018) introduced an adversarially trained agent that is trained via a reinforcement learning setup without any supervision to generate a program that is executed by a graphics engine to interpret and sample images. In contrast, our work presents two complementary rewards (one in image space and another in specification space) in a reinforcement learning setup for the image de-rendering problem.

3 Models

Task. For each task we consider, there is a simple graphics specification language that can be used to specify a particular image. While differing in details, the overall scheme of the specifications are the same for each. A specification consists of a set of “objects”, and each object is specified by a set of properties. Examples of an object specification for each of our tasks can be seen in Fig. 1. Given an image rendered from a specification, our task is to “de-render” this image back to the original specification. We can evaluate a predicted specification by looking for exact matches between the objects in the predicted specification and the objects in the original specification. We can summarize the object matches with standard measures, such as precision, recall, F1, and intersection-over-union. While these measures describe performance on a single image, we can average these measures across a collection of images, to get a performance measure of a method overall. We provide more details in Sec. 5.2. Another approach to evaluation is to generate the image corresponding to a predicted specification, and see how well it matches the original image, using some reasonable metric on the space of images.

Reduction to sequence prediction. While each specifications is represented by a set of objects with specific properties, our models require sequences of tokens. We convert the set of objects to a sequence of tokens via some ordering of the objects. We investigate various approaches to ordering (Sec. 7.1), and find that ordering by object type works best. Once the model predicts a sequence of tokens, we can parse it back into original structure to compute performance measures and our reward functions for reinforcement learning.

3.1 Image-to-LSTM Sequence Model

Our baseline model is similar to an image captioning model with an attention mechanism (Xu et al. 2015). We use the ResNet-18 architecture (He et al. 2016) for encoding the input image, and we use an LSTM-RNN for predicting the corresponding specification as a sequence of tokens.

We will denote the convolutional features from the ResNet-18 as $\{f_i\}_{i=1}^m$, where $f_i \in \mathbb{R}^d$. For any decoder output token o , let $E_o \in \mathbb{R}^d$ denote its embedding, which will be learned during training. Let s_t be the decoder state at step t , o_t be the output token at step t , and c_t be the image context vector at step t , which will be defined below. Then at step t , the decoder state s_t is given by

$$s_t = \mathbb{F}(c_t, s_{t-1}, E_{o_{t-1}}), \quad (1)$$

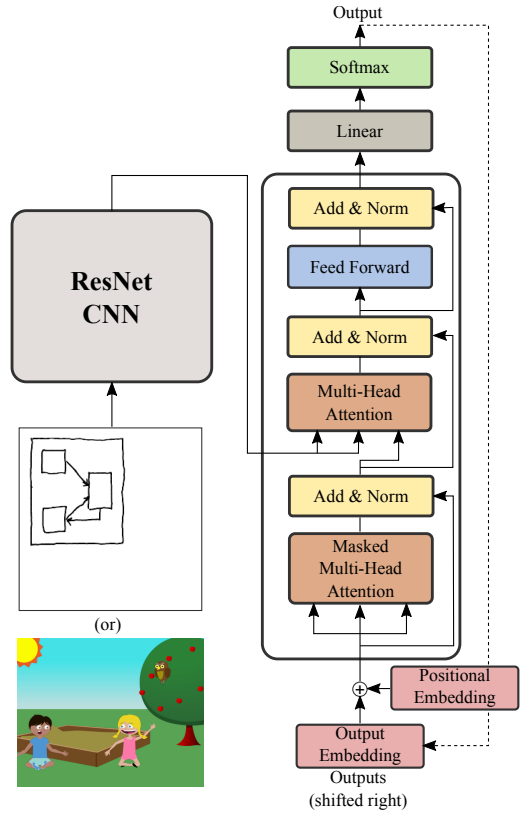


Figure 2: Our Image-Transformer model.

where \mathbb{F} is a trainable non-linear function. The context vector c_t is a convex combination of the image features: $c_t = \sum_{i=1}^m \alpha_{t,i} f_i$, where $\alpha_{t,i}$ are “attention weights” defined as

$$\alpha_{t,i} = \frac{\exp(e_{t,i})}{\sum_{k=1}^m \exp(e_{t,k})} \quad (2)$$

$$e_{t,i} = v^T \tanh(W f_i + U s_{t-1} + b), \quad (3)$$

where v , W , U , and b are the trainable parameters.

3.2 Image-to-Transformer Sequence Model

Recently, there is an increasing amount of interest in Transformer networks (Vaswani et al. 2017), which are said to train faster and to better capture long-term dependencies than LSTM-based RNN models. In our specification prediction problem, the length of the specification can be large, and we need long-term dependencies to avoid generating objects that have already been generated. This suggests Transformer networks would be a better fit for our scenario. In this work, we only use the decoder part of the Transformer network (Vaswani et al. 2017). The Transformer encoder is for use on sequences, and we replace it with ResNet-18 CNN described above. We give a high-level description of the Transformer decoder below, and refer to Vaswani et al. (2017) for full details.

The decoder of the Transformer has a stack of N identical layers containing self-attention modules, normalization modules, and feed-forward modules, along with posi-

tional encoding module for output embeddings (see Fig. 2). While the original model in Vaswani et al. (2017) took $N=6$, through hyperparameter tuning we found $N=4$ to work better for our problem. Besides that, we used the hyperparameter settings as in Vaswani et al. (2017). The decoder has two attention modules: one for attending to the image convolution features and another self-attention module to attend to different previous positions in the decoder state.

Attention in Transformer. As shown in Fig. 2, we have two attention mechanisms in the model: one attending to the CNN features, and another attending to different parts of the decoder state. They all have the same structure, which we describe below.

An attention mechanism in the Transformer can be viewed as a mapping from a query (Q) and a key-value (K, V) pair to an output. An attention weight is computed using the query and key and those weights are used with values to compute the output of the attention module. Empirically, it has been proven that instead of performing a single attention function, linearly projecting the queries, keys, and values with different learned projection layers and then performing the attention function in parallel and concatenating those outputs to get the final attention module output to work better. This attention mechanism is called multi-head attention mechanism (MH), which is defined as follows:

$$\text{MH}(Q, K, V) = \text{Concat}(\text{head}_1, \dots, \text{head}_h)W^O \quad (4)$$

$$\text{head}_i = \text{Attention}(QW_i^Q, KW_i^K, VW_i^V) \quad (5)$$

$$\text{Attention}(Q, K, V) = \text{softmax}\left(\frac{QK^T}{d_k}\right)V \quad (6)$$

where, d_k is the dimension of the queries and keys, W_i^Q , W_i^K , and W_i^V are the parameters of the projection matrices.

Position-wise Feed-Forward Networks. In addition to the attention sub-layers, each of the layers in the Transformer decoder contains a fully connected feed-forward network that is applied to each position of the decoder separately and identically. This network is defined as

$$\text{FFN}(x) = \max(0, xW_1 + b_1)W_2 + b_2, \quad (7)$$

where W_1 , W_2 , b_1 , and b_2 are the linear projection parameters which are same across different positions but are different from layer to layer.

Positional Encoding. In the model described thus far, the model is symmetric with respect to sequence position. For example, at the bottom right of Fig. 2, the model has no structural way to determine which output embeddings come from which part of the output sequence. To remedy this issue, we concatenate a ‘‘positional encoding’’ (PE) to the embedding representation of the tokens. We use the sine and cosine functions for positional encoding:

$$\text{PE}(\text{pos}, 2i) = \sin(\text{pos}/10000^{2i/d_{\text{model}}}) \quad (8)$$

$$\text{PE}(\text{pos}, 2i + 1) = \cos(\text{pos}/10000^{2i/d_{\text{model}}})$$

where pos is the position, i is the dimension, and d_{model} is the dimension of the embedding vector representation.

4 Dual-Modality Two-Way Reinforcement Learning

Traditionally, sequence generation models are trained using a cross-entropy loss. More recently, a policy gradient-based reinforcement learning approach has been explored for sequence generation tasks (Ranzato et al. 2016; Rennie et al. 2017), which has two advantages over the cross-entropy loss optimization approach: (1) avoiding the *exposure bias* issue, which is about the imbalance in the output distributions created by different train and test time decoding approaches in cross-entropy loss optimization (Bengio et al. 2015; Ranzato et al. 2016); (2) allows direct optimization of the evaluation metric of interest, even if it is not differentiable. To this end, we use a policy gradient-based approach via rewards in both the specification space and the image space. Also, we explore joint rewards based on these two spaces for better capturing feedback that is complementary between these two modalities.

For this reward optimization, we use the REINFORCE algorithm (Williams 1992; Zaremba and Sutskever 2015) to learn a policy p_θ that produces a distribution over sequences o^s for any given input. We try to find a policy p_θ such that the expected reward for a label sequence o^s drawn according to the predicted distribution has maximum expected reward. Equivalently, we minimize the following loss function, in average across all training inputs:

$$L_{\text{RL}} = -\mathbb{E}_{o^s \sim p_\theta}[r(o^s)], \quad (9)$$

where o^s is the sequence of sampled tokens with o_t^s sampled at time step t of the decoder. We can approximate the gradient of this loss function with respect to the parameter θ using a single sample o^s drawn from p_θ as:

$$\nabla_\theta L_{\text{RL}} = -(r(o^s) - b_e)\nabla_\theta \log p_\theta(o^s), \quad (10)$$

where the leading factor is included for variance reduction using a baseline estimator (Zaremba and Sutskever 2015). There are several ways to calculate the baseline estimator; we employ the effective SCST approach (Rennie et al. 2017).

4.1 Rewards

In this work we consider three different reward functions. Two of the rewards are based in ‘‘specification space’’, which make a direct comparison between the predicted specification and the ground truth specification, and one of the rewards is based in ‘‘image space’’, which compares the image rendered from the predicted specification with original input image. We also investigate using these rewards in combination, with the hope that there is complementary information in the feedback based on the two spaces.

Intersection-Over-Union Reward (IOU) As mentioned in Sec. 3, after the specification is predicted as a sequence of tokens, we can parse the sequence into a set of object specifications. The intersection-over-union (IOU) reward is based in specification space. Roughly speaking, the IOU reward gives credit for predicting objects that exactly match objects in the ground truth specification, and penalizes both

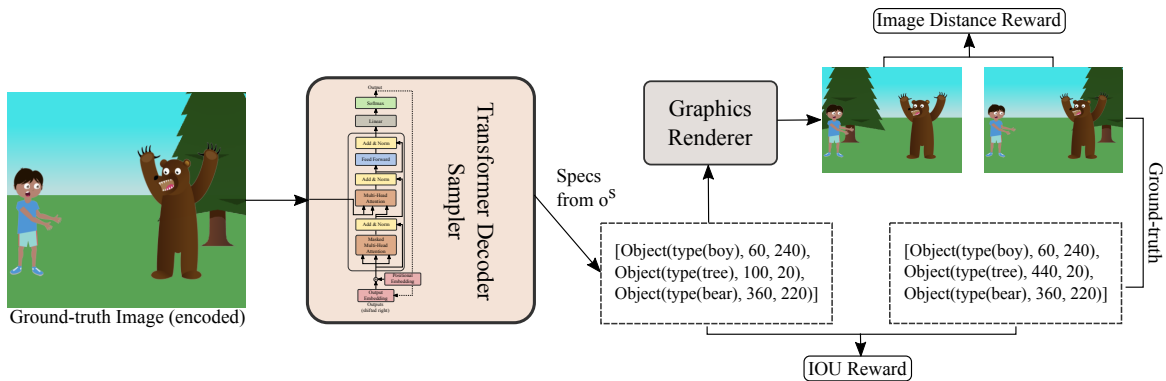


Figure 3: Example showing the samples from our model based on abstract scene dataset and the corresponding rewards in specification and image space. For simplicity, all object properties are not shown in specification space.

for predicting objects that do not match ground truth objects and for failing to predict objects that are part of the ground truth. More formally, let $\{o_i\}_{i=1}^m$ and $\{o_j^*\}_{j=1}^n$ represent the objects in predicted and ground-truth specifications, respectively. Then the IOU reward is defined as:

$$r_{iou} = \frac{\text{count}(\{o_i\}_{i=1}^m \cap \{o_j^*\}_{j=1}^n)}{\text{count}(\{o_i\}_{i=1}^m \cup \{o_j^*\}_{j=1}^n)} \quad (11)$$

The object o_i in the prediction specification is the same as object o_j^* in the ground-truth specification if and only if all the properties of these objects match exactly.

Inference Reward Our second reward, which we call the “inference reward”, is also a reward in specification space. The name is based on the “inference error”, which is a performance measure introduced in Wu, Tenenbaum, and Kohli (2017) for the Abstract Scenes dataset. While IOU is based on exact matches between predicted objects and ground-truth objects, the inference error and inference reward are based on the number of properties (within objects) that correctly match the corresponding properties in the ground-truth. For those properties specifying location in pixel coordinates, we follow Wu, Tenenbaum, and Kohli (2017) and divide the space of each coordinate into 20 bins of equal size, and we consider it a match if the predicted and ground-truth locations are in the same bin. We define the inference error as the fraction of predicted properties that fail to match the corresponding ground-truth properties. The inference reward is one minus the inference error.

Image Distance Reward Our third and final reward, the “image distance reward”, is in image space. We define it generically first, as it takes slightly different forms in our two datasets. If we let I and I^R represent vectorized versions of the input image and the image rendered from the predicted specification, respectively, then we define the image distance as

$$d_{img} = \|I \ominus \Psi(I^R)\|_2^2, \quad (12)$$

where $\|\cdot\|_2$ is the ℓ_2 -norm.

For Noisy Shapes dataset, we follow Ellis et al. (2018) and take Ψ to be a Gaussian blurring function, as the objects

in the target image have noise (see Fig. 1). We take \ominus to be a simple subtraction operation. The image reward for this dataset is:

$$r_{img} = \frac{c}{d_{img}} \quad (13)$$

where c is a tunable parameter.

For the Abstract Scene dataset, \ominus is a logical operator that takes the value 0 in every position where the pixel values “match”, and 1 in every other position. The range of possible pixel values is 0-255 and, similarly to the discretization of position in the inference reward, we divide the pixel value range into 20 equisized buckets and consider pixel values to match if they are in the same bucket. We take Ψ to be the identity function. The image reward for the Abstract Scenes dataset is then defined as:

$$r_{img} = 1 - \frac{d_{img}}{w \cdot h} \quad (14)$$

where w and h are width and height of the image.

Joint Dual-Modality Reward Since we expect the rewards based in specification space to be complementary to the reward based in image space, we want a way to combine rewards on the two spaces. One way to combine two rewards is to create a weighted combination of individual rewards to formulate the joint reward. Another approach is to alternate the reward used during the learning process (Pasunuru and Bansal 2018). In this work, we follow the latter approach, as the former approach requires expensive tuning for scale and weight balancing. Let r_1 and r_2 be the two reward functions that we want to optimize. In our approach, we first take a_1 optimization steps to minimize the reinforcement learning loss $L_{RL_1}(r_1; \theta)$ (i.e. we use a_1 mini-batches). Then we take a_2 optimization steps to minimize the reinforcement learning loss $L_{RL_2}(r_2; \theta)$. We then repeat this cycle of steps until convergence. All other optimization parameters, such as step size, remain the same for each set of steps. The values a_1 and a_2 are tuning parameters.³ The two rewards r_1 and r_2 could be based on different aspects of the output, such as IOU and image distance reward.

³Pasunuru and Bansal (2018) set a_1 and a_2 to 1, without tuning.

Model	Precision	Recall	F1	IOU	IOU _{1.0}	IOU _{0.8}	IOU _{0.6}
CROSS-ENTROPY LOSS							
Image2LSTM+atten.	98.7	98.5	98.6	97.6	90.7	95.3	98.8
Image2Transformer	99.1	99.1	99.1	98.5	94.1	97.3	99.1
IMAGE2TRANSFORMER WITH REINFORCE LOSS							
IOU Reward	99.4	99.3	99.3	98.8	95.0	98.0	99.4
Image-distance Reward	99.4	99.2	99.3	98.8	94.5	98.0	99.5
Image-distance + IOU Reward	99.4	99.3	99.3	98.8	95.0	98.1	99.4

Table 1: Performance of various models on Noisy Shapes dataset.

5 Experimental Setup

5.1 Dataset

Noisy Shapes Dataset. Ellis et al. (2018) provides a synthetic dataset of images containing multiple simple objects (lines, circles, and rectangles), each with various properties that can be specified. The images are specified using a small subset of \LaTeX drawing commands. Additional noise is introduced into the rendered images by rescaling image intensity, translating the image by a few pixels, rendering the \LaTeX using the pencildraw style, and randomly perturbing the position and sizes of these \LaTeX drawing commands. The dataset was created by randomly sampling image specifications with between 1 and 12 objects, excluding any specifications that lead to images with overlapping objects. The size of each image is 256x256. The dataset contains 100,000 images paired with specifications, from which we use 1000 for testing and the rest for training.

Abstract Scene Dataset. The Abstract Scene dataset (Zitnick and Parikh 2013) contains 10,020 images, each of which has 3-18 objects. There are over 100 types of objects, each of which is specified by two integers, one indicating a broad category (e.g. sky object, animal, boy, girl) and another indicating a subcategory (e.g. girl pose, animal type, etc.). Each object can be drawn at one of 3 scales, with or without a horizontal flip, and at any pixel location in the 500x400 image. These properties are specified by 4 additional integers. Thus each object is specified by 6 integers. There are often heavy occlusions among these objects when rendered in an image (see input image in Fig. 2). However, the objects are rendered in a deterministic order based on the object types and other properties, and thus the image is independent of the order of the objects in the specification. Similar to Wu, Tenenbaum, and Kohli (2017), we randomly sample 90% of the images for training and rest for testing.

5.2 Evaluation Metrics

Noisy Shapes Dataset. As described in the Task description of Sec. 3, we can summarize performance on a single image with precision, recall, F1, and IOU (intersection over union) at the object level. Following previous work (Ellis et al. 2018), we summarize the performance of a method by averaging these metrics across all test examples (i.e. a

macro average). Further, we also report IOU_k , which is defined as the percent of test examples for which the IOU score is greater than or equal to k .

Abstract Scene Dataset. For the abstract scene dataset, following previous work (Wu, Tenenbaum, and Kohli 2017), we report specification inference error and image reconstruction error based on a micro average across all test examples. As described in Sec. 4.1 and Sec. 4.1, inference error is based on the percentage of incorrectly inferred values (i.e., how many properties of objects do not match with the ground-truth) for the specification, and image reconstruction error is based on percentage of incorrect pixel prediction. During these evaluations, all the continuous variables (pixel values, and x and y coordinates) are quantized into 20 bins. Additionally, we report the macro average based IOU error as described for the noisy shapes dataset.

5.3 Training Details

In all of our models, we encode the image information via ResNet-18 (He et al. 2016), where we take the penultimate layer’s features as outputs from this image encoder. For LSTM-RNN, we use a hidden state size of 128, input token embedding size of 128, and a batch size of 64. For Transformer networks, we use the same hidden and embedding size, and use 4 layers at each time step. We use the Adam optimizer (Kingma and Ba 2015) with the default learning rate of 0.001 for all the cross-entropy models, and a learning rate of 0.0001 for all the reinforcement learning based models. For the Noisy Shapes dataset, the maximum decoder length is fixed to 80, and we use a vocabulary size of 27, which are placeholders for object properties. For the Abstract Scene dataset, the maximum decoder length is fixed to 100, and we use a vocabulary size of 1078 which represents all the object properties. For the joint reward optimization, we use a mixing ratio of 1:1 for the Noisy Shapes dataset and 1:4 for the Abstract Scene dataset.

6 Results

6.1 Results on the Noisy Shapes Dataset

We first compare the performance of the LSTM-RNN model (Image2LSTM+atten) to the Transformer-based model, when both are trained with cross-entropy loss. We see in

Model	Infer. Error	Recons. Error	Avg. Error	IOU
PREVIOUS WORK				
CNN+LSTM (2017)	45.31	41.38	43.84	-
NSD (full) (2017)	42.74	21.55	32.14	-
CROSS-ENTROPY LOSS				
Image2LSTM+atten.	17.27	15.70	16.48	32.06
Image2Transformer	8.78	10.92	9.85	58.54
IMAGE2TRANSFORMER WITH REINFORCE LOSS				
IOU Reward	7.91	10.50	9.20	61.29
Inference Reward	7.81	10.75	9.28	59.35
Recons. Reward	8.34	9.99	9.16	62.44
Inference + Recons.	8.21	10.12	9.16	61.54
IOU + Recons.	8.05	10.04	9.04	62.45

Table 2: Models performance on the abstract scene dataset. Errors: lower is better; IOU: higher is better.

Table 1 that the Transformer model dominates on all measures. In particular, we highlight $\text{IOU}_{1,0}$, which measures the percent of examples on which the predicted specification exactly matches the ground-truth specification. While the LSTM-RNN model achieves a 90.7% $\text{IOU}_{1,0}$, the Transformer model achieves 94.1%, which is an impressive 36.5% reduction in the number of errors. We have similar performance improvements for the other metrics. We now compare the Transformer model trained with reinforcement learning, using various reward functions, to training using cross-entropy loss. Table 1 shows that, although all three reward variations have roughly the same performance, they all show significant improvement over cross-entropy training, on all measures.⁴ For example, the model trained with IOU reward achieved a 95.0% $\text{IOU}_{1,0}$ measure, which is an impressive 15.3% reduction in the number of errors compared to the same model trained with cross-entropy loss, and a 46.2% reduction compared to the original LSTM-RNN model. Performance improvement in the other measures is at least as good.

6.2 Results on Abstract Scene Dataset

In Table 2, we see the performance of various models on the Abstract Scene dataset, for the metrics described in Sec. 5.2. We first note that even our baseline LSTM-RNN model (Image2LSTM+atten) shows a very large error reduction compared to the results presented in Wu, Tenenbaum, and Kohli (2017) (first 4 rows of the table). This highlights the importance of an attention mechanism in these tasks. For the models trained with cross-entropy, the Transformer model shows an additional remarkable improvement over the LSTM-RNN model, across all measures.

For reinforcement learning with the Transformer model,

⁴The improvement of our Transformer models trained with reinforcement learning over the corresponding cross-entropy models is statistically significant with $p < 0.01$, based on the bootstrap test (Noreen 1989; Efron and Tibshirani 1994).

we tried three different reward functions, corresponding to three of our performance metrics: inference error, reconstruction error, and IOU. All the Transformer models trained with REINFORCE out-performed the model trained with cross-entropy loss for each of the error measures.⁵ For inference error, the model trained with the inference reward did the best, as one might hope and expect. Compared to the cross-entropy trained Transformer, the inference error measure was reduced by 11.0%. For reconstruction error (image-based), the best performing model was the model trained with the reconstruction reward, which reduced the reconstruction error by 8.5% compared to the cross-entropy trained version. When evaluating performance using the average of the inference and reconstruction error, one of our joint-reward models performed best, though interestingly, not the one that uses the corresponding inference and reconstruction rewards. The best performing model for this performance measure used IOU and reconstruction rewards, suggesting that IOU reward has more information that is complementary to the reconstruction error than does the inference reward. For IOU performance measure, the model trained with IOU reward did well, but when trained jointly with IOU and reconstruction reward, it performed the best. This suggests that using image-based feedback during training (recons. error) can be beneficial even when the ultimate goal (IOU) depends only on the specification output.

7 Analysis

7.1 LSTM vs. Transformer Networks

As noted above, for the Abstract Scene and the Noisy Shapes datasets that we consider, the order of the objects in the specification does not affect the final image. Nevertheless, for training both the LSTM-RNN and the Transformer models, one must choose an ordering. We ran an experiment using the Noisy Shapes dataset, in which we tried ordering the objects by shape size, shape type, and by shape position in the rendered image. We found that ordering by shape type worked best across our models, so that’s what we used for our main results in Table 1. We also wanted to investigate how important it is to have the objects in some sensible order, compared to a random ordering. Table 3 shows the results of our two models when trained with cross-entropy on specification sequences where the objects are put in random order. We find that the LSTM-RNN model performance drops dramatically (e.g. $\text{IOU}_{1,0}$ drops from 90.7% to 72.0%), while the drop with Transformer networks is quite small (e.g. $\text{IOU}_{1,0}$ drops from 94.1% to 93.2%).⁶ This is addi-

⁵For the IOU and inference reward models, this improvement is statistically significant for all metrics except reconstruction error. For the reconstruction reward model, the improvement is significant for all but the inference error metric. For the dual (IOU+Recons.) reward model, the difference is significant for all metrics ($p < 0.01$ for each test).

⁶Note that the number of model parameters is approximately the same (11.8M for Transformer model and 11.5M for LSTM model). Further, Transformer models are 2.5x faster to train in comparison to the LSTM models. During inference, both models take approximately the same time.

Model	F1	IOU	IOU _{1.0}
Image2LSTM+atten.	95.2	92.0	72.0
Image2Transformer	99.0	98.3	93.2

Table 3: Performance of LSTM-RNN and Transformer networks on the Noisy Shapes dataset when specifications have randomly ordered objects.

tional evidence for Transformers being the preferred model for tasks of this type.

7.2 Performance vs. Data Size

We conduct an experiment where we vary the percentage of Noisy Shapes data used during our models’ training from 10% to 100% by steps of 20%. We observe that with less data (10%-40%), the RL-based model is approximately 2 points better (on the IOU_{1.0} metric) than its corresponding cross-entropy baseline. As we use more data (>60%), the gap decreases to 1 point between RL and cross-entropy models. This suggests that RL, which has the advantage of exploration, is more powerful when the data is less.

7.3 Output Examples

Fig. 4 presents the output rendered images of the predicted specifications from Image2Transformer cross-entropy model and the corresponding RL-based model with IOU+Image-distance as reward for noisy shapes dataset and IOU+Recons. as reward for abstract scene dataset. In the first example (top row in Fig. 4), the cross-entropy model predicts an extra ‘line shape’ which is not present in the ground-truth. Our RL model correctly predicts the exact same shapes present in the ground-truth. However, neither models getting the type of ‘line shape’ correct in couple of instances. In the second example (second row in Fig. 4), the cross-entropy model predicts an extra object (glasses), which is not present in the ground-truth image, and is also missing the cap on the snake. The RL model improves on the cross-entropy model by not having any extra objects, but it is also missing the cap. In the third example, both the rendered images look very similar to the ground-truth, but the cross-entropy model predicts one of the objects (glasses) slightly off in position. Our RL model was able to accurately position the glasses (bottom row in Fig. 4). The better performance of RL model may be due to the image space component of the error signal, which is more sensitive to position errors, while the cross-entropy loss gives the same penalty to all incorrect positions regardless of the error size.

8 Conclusion

We present various neural de-rendering models based on LSTMs with attention mechanism and Transformer networks. Further, we introduce complimentary dual rewards (one in specification space and another in image space) and optimize them via reinforcement learning, and achieve state-of-the-art results. Further, our results and analyses suggest

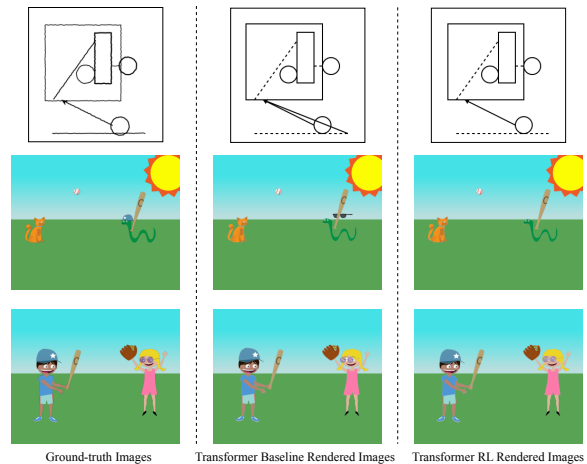


Figure 4: Comparing the ground-truth images from noisy shapes and abstract scene datasets with the rendered images of predicted specifications.

that Transformers are a better choice than LSTMs for unordered sequence prediction tasks.

Acknowledgments

We thank the reviewers for their helpful comments. This work was partially supported by NSF-CAREER Award 1846185, ARO-YIP Award W911NF-18-1-0336, and a Microsoft PhD Fellowship. The views contained in this article are those of the authors and not of the funding agency.

References

- Bengio, S.; Vinyals, O.; Jaitly, N.; and Shazeer, N. 2015. Scheduled sampling for sequence prediction with recurrent neural networks. In *Proceedings of the 28th International Conference on Neural Information Processing Systems - Volume 1*, NeurIPS’15, 1171–1179. Cambridge, MA, USA: MIT Press.
- Bluche, T.; Louradour, J.; and Messina, R. O. 2016. Scan, attend and read: End-to-end handwritten paragraph recognition with MDLSTM attention. *CoRR* abs/1604.03286.
- Bunel, R.; Hausknecht, M.; Devlin, J.; Singh, R.; and Kohli, P. 2018. Leveraging grammar and reinforcement learning for neural program synthesis. In *ICLR*. OpenReview.net.
- Chen, X.; Fang, H.; Lin, T.-Y.; Vedantam, R.; Gupta, S.; Dollár, P.; and Zitnick, C. L. 2015. Microsoft COCO captions: Data collection and evaluation server. *CoRR* abs/1504.00325.
- Cliche, M.; Rosenberg, D.; Madeka, D.; and Yee, C. 2017. Scatteract: Automated extraction of data from scatter plots. In *Joint European Conference on Machine Learning and Knowledge Discovery in Databases*, 135–150. Springer.
- Daumé, H.; Langford, J.; and Marcu, D. 2009. Search-based structured prediction. *Machine Learning* 75(3):297–325.
- Deng, Y.; Kanervisto, A.; Ling, J.; and Rush, A. M. 2017. Image-to-markup generation with coarse-to-fine attention.

- In *Proceedings of the 34th International Conference on Machine Learning - Volume 70*, ICML'17, 980–989. JMLR.org.
- Efron, B., and Tibshirani, R. J. 1994. *An introduction to the bootstrap*. Number 57 in Monographs on Statistics and Applied Probability. Boca Raton, Florida, USA: Chapman & Hall/CRC.
- Ellis, K.; Ritchie, D.; Solar-Lezama, A.; and Tenenbaum, J. B. 2018. Learning to infer graphics programs from hand-drawn images. In *Proceedings of the 32nd International Conference on Neural Information Processing Systems*, NeurIPS'18, 6062–6071. Red Hook, NY, USA: Curran Associates Inc.
- Ganin, Y.; Kulkarni, T.; Babuschkin, I.; Eslami, S. M. A.; and Vinyals, O. 2018. Synthesizing programs for images using reinforced adversarial learning. In *Proceedings of the 35th International Conference on Machine Learning*.
- Ha, D., and Eck, D. 2018. A neural representation of sketch drawings. In *6th International Conference on Learning Representations, ICLR 2018, Vancouver, BC, Canada, April 30 - May 3, 2018, Conference Track Proceedings*. OpenReview.net.
- He, K.; Zhang, X.; Ren, S.; and Sun, J. 2016. Deep residual learning for image recognition. In *CVPR*, 770–778.
- Huang, H.; Kalogerakis, E.; Yumer, E.; and Mech, R. 2016. Shape synthesis from sketches via procedural models and convolutional networks. *IEEE Transactions on Visualization and Computer Graphics 2*.
- Karpathy, A., and Fei-Fei, L. 2015. Deep visual-semantic alignments for generating image descriptions. In *Proceedings of the IEEE conference on computer vision and pattern recognition*, 3128–3137.
- Kingma, D. P., and Ba, J. 2015. Adam: A method for stochastic optimization. In Bengio, Y., and LeCun, Y., eds., *3rd International Conference on Learning Representations, ICLR 2015, San Diego, CA, USA, May 7-9, 2015, Conference Track Proceedings*.
- Lin, T.; Maire, M.; Belongie, S. J.; Bourdev, L. D.; Girshick, R. B.; Hays, J.; Perona, P.; Ramanan, D.; Dollár, P.; and Zitnick, C. L. 2014. Microsoft COCO: common objects in context. *CoRR* abs/1405.0312.
- Liu, Y.; Wu, Z.; Ritchie, D.; Freeman, W. T.; Tenenbaum, J. B.; and Wu, J. 2019. Learning to describe scenes with programs. In *ICLR*.
- Mishchenko, A., and Vassilieva, N. 2011. Chart image understanding and numerical data extraction. In *2011 Sixth International Conference on Digital Information Management*, 115–120. IEEE.
- Nishida, G.; Garcia-Dorado, I.; Aliaga, D. G.; Benes, B.; and Bousseau, A. 2016. Interactive sketching of urban procedural models. *ACM Transactions on Graphics (TOG)* 35(4):130.
- Noreen, E. W. 1989. *Computer-intensive methods for testing hypotheses*. Wiley New York.
- Pasunuru, R., and Bansal, M. 2018. Multi-reward reinforced summarization with saliency and entailment. In *Proceedings of the 2018 Conference of the North American Chapter of the Association for Computational Linguistics: Human Language Technologies, Volume 2 (Short Papers)*, 646–653.
- Paulus, R.; Xiong, C.; and Socher, R. 2018. A deep reinforced model for abstractive summarization. In *6th International Conference on Learning Representations, ICLR 2018, Vancouver, BC, Canada, April 30 - May 3, 2018, Conference Track Proceedings*. OpenReview.net.
- Ranzato, M.; Chopra, S.; Auli, M.; and Zaremba, W. 2016. Sequence level training with recurrent neural networks. In *ICLR*.
- Rennie, S. J.; Marcheret, E.; Mroueh, Y.; Ross, J.; and Goel, V. 2017. Self-critical sequence training for image captioning. In *IEEE Conference on Computer Vision and Pattern Recognition*, 1179–1195.
- Sharma, P.; Ding, N.; Goodman, S.; and Soricut, R. 2018. Conceptual captions: A cleaned, hypernymed, image alt-text dataset for automatic image captioning. In *Proceedings of the 56th Annual Meeting of the Association for Computational Linguistics (Volume 1: Long Papers)*, 2556–2565.
- Sun, S.-H.; Noh, H.; Somasundaram, S.; and Lim, J. 2018. Neural program synthesis from diverse demonstration videos. In *International Conference on Machine Learning*, 4797–4806.
- Vaswani, A.; Shazeer, N.; Parmar, N.; Uszkoreit, J.; Jones, L.; Gomez, A. N.; Kaiser, Ł.; and Polosukhin, I. 2017. Attention is all you need. In *NeurIPS*, 5998–6008.
- Vinyals, O.; Bengio, S.; and Kudlur, M. 2015. Order matters: Sequence to sequence for sets. In *ICLR*.
- Williams, R. J. 1992. Simple statistical gradient-following algorithms for connectionist reinforcement learning. *Machine learning* 8(3-4):229–256.
- Wu, J.; Tenenbaum, J. B.; and Kohli, P. 2017. Neural scene de-rendering. In *Proceedings of the IEEE Conference on Computer Vision and Pattern Recognition*, 699–707.
- Xu, K.; Ba, J.; Kiros, R.; Cho, K.; Courville, A.; Salakhudinov, R.; Zemel, R.; and Bengio, Y. 2015. Show, attend and tell: Neural image caption generation with visual attention. In *ICML*, 2048–2057.
- Zaremba, W., and Sutskever, I. 2015. Reinforcement learning neural Turing machines. *arXiv preprint arXiv:1505.00521*.
- Zhou, L.; Zhou, Y.; Corso, J. J.; Socher, R.; and Xiong, C. 2018. End-to-end dense video captioning with masked transformer. In *Proceedings of the IEEE Conference on Computer Vision and Pattern Recognition*, 8739–8748.
- Zitnick, C. L., and Parikh, D. 2013. Bringing semantics into focus using visual abstraction. In *Proceedings of the IEEE Conference on Computer Vision and Pattern Recognition*, 3009–3016.